Three-Dimensional Structure of the Zone-Drawn Film of the Nylon-6/ Layered Silicate Nanocomposites

Soo-Young Park,*,† Yang-Hwan Cho,† and Richard A. Vaia‡

Department of Polymer Science, Kyungpook National University, #1370 Sangyuk-dong, Buk-gu, Daegu 702-701, Korea, and Air Force Research Laboratory, Materials and Manufacturing Directorate, Wright-Patterson AFB, Ohio 45433-7750

Received August 24, 2004; Revised Manuscript Received November 19, 2004

ABSTRACT: Semicrystalline polymer/layered silicate nanocomposites exhibit a unique three-dimensional structure associated with the high-aspect ratio constituents (layered silicates and polymer crystallites), which is sensitive to shear and deformation history. Beginning from quenched biaxially extruded films of nylon-6/ montmorillonite nanocomposites, the impact of elevated temperature uniaxial drawing on the orientation of the layered silicate and crystallites, crystalline polymorphism, and layered silicate buckling was studied using X-ray and transmission electron microcopy. The quenched biaxially protruded films exhibited a uniplanar crystalline texture with the *b*-axis of the dominate γ-form oriented toward the normal to the film surface and the surface of the layered silicate oriented parallel to the film surface. Small-angle scattering features suggest that the lamellar of the γ-form is within the proximity of the layered silicate and has a fringed micelle structure. Upon uniaxial drawing, α-crystallites developed with a lamellar regularity of ∼15 nm along the draw direction, comparable to previous studies on pure nylon-6 fibers. The newly formed α-form exhibited a uniaxial texture with the *b*-axis parallel to the draw direction. This suggests that the α-form crystallized during the drawing of the film and does not have an orientation correlation with the layered silicate. Finally, the layered silicate within the zone-drawn film buckled perpendicular to the draw direction, analogous to failure of a uniaxially strained sheet of paper. The failure mode appears to occur for a collection of parallel aluminosilicate layers (2−4) and not individually. Recognition of the structural changes of the layered silicate and crystalline regions in response to uniaxial deformation of planar oriented films is critical to ascertaining the local transport properties of shaped layered silicate nanocomposite parts.

Introduction

In contrast to traditional filled or fiber-reinforced polymer systems, several new thermoplastic nanocomposites have recently been developed.[1] One notable example is the nylon-6/layered silicate nanocomposites (NCH) which has gained much attention since Toyota researchers first demonstrated a stunning improvement of its mechanical properties as compared to the pristine nylon-6. Most notable is the unexpected suite of property enhancements obtained from the addition of a few wt % layered silicate, such as the retention of impact strength, increased atomic oxygen resistance, and an improved ablative performance. The exfoliation of individual, 1 nm thick aluminosilicate layers in the NCH system was achieved through a high-temperature ring-opening polymerization of ϵ-caprolactams, initiated from aminolauric acid modifiers on the layered silicate surface.[2−4] Following, numerous polyamide nanocomposite systems have been developed, including the ability to directly form the NCH by melt processing of the organically modified layered silicate with the resin. From a processing perspective, these NCH systems are very practical, being amenable to injection molding or extrusion.[5−13]

Substantial fundamental efforts have been devoted to understanding the reinforcing mechanism and impact on crystal phase development of nylon-6 by the layered silicate. In general, low volume percent (1−5 vol %) addition of layered silicate impacts polymer crystallite development, having been observed in the vast majority of investigations on semicrystalline polymer nanocomposites. General effects include induced polymorphism,[14−21] small, irregular crystallites (dendrites, hedrites),[22−25] increased crystallization rate,[9,17,18,26−30] and alteration of the crystal fraction.[31−33] The extent of these effects depends on process history and specific characteristics of the resin. Nylon-6 nanocomposites have been the most extensively studied semicrystalline nanocomposite to date, greatly facilitated by the substantial investigations available on the unfilled polymer.

Nylon-6 commonly exhibits two room temperature crystalline forms, γ and α, where α is thermodynamically favored. Brill et al.[34] and Holmes et al.[35] determined the α-form in a fiber specimen, consisting of a monoclinic unit cell (a = 9.56 Å, b = 17.24 Å, c = 8.01 Å, β = 67.5°) where the b dimension is along the fiber axis. There are eight monomeric units in the unit cell with an extended-chain sheet structure and hydrogen bonding between adjacent antiparallel chains. Homes et al.[35] and Arimoto et al.[36] also determined the γ-form of nylon-6, consisting of a monoclinic unit cell (a = 9.33 Å, b = 16.88 Å, c = 4.78 Å, β = 121°) with the b dimension being along the fiber axis. Bardbury et al. proposed the metrically pseudo-orthorhombic cell with a = 4.82 Å, b = 7.82 Å, and c = 16.7 Å (chain axis),[37] which is similar to the first one.[35,36] The first unit cell of γ is used in this paper. This form has four monomeric units in the unit cell and hydrogen bonding between parallel chains. The γ-form is often associated with the formation of extended chain crystals and is typically obtained from a process involving elongational flow,

† Kyungpook National University.
‡ Air Force Research Laboratory.
* To whom correspondence should be addressed: Tel +82-53-950-5630; Fax +82-53-950-6623; e-mail psy@knu.ac.kr.

10.1021/ma048258n CCC: $30.25
Published on Web 02/02/2005

such as fiber spinning.[38] With axial tension it can be converted into the α-form by annealing[39] or by treating nylon-6 with a phenolic aqueous solution.[40,41] The addition of layered silicate has been shown to favor the formation of the metastable γ-form.[7,8,42−44] The polymorphism is independent of preparation methods, including in-situ polymerization[7,8,43] and melt intercalation with various organically modified[42,44] and silane-treated clays. Lincoln et al. concluded that the γ-form is preferentially in the proximity of the silicate layers, whereas the α-form exists away from the polymer−silicate interphase region.[19]

Ascertaining the synergism between the orientation of the high aspect ratio layered silicate and the development of crystal phase morphology during film or fiber processing is paramount to enabling many applications for NCHs. For example, it is known that the film drawing of NCH is quite difficult due to the strong interaction between the layered silicate and the polymer matrix. Kojima and co-workers initially studied the orientation of montmorillonite and nylon-6 crystallites in the NCH film, which revealed that the silicate layers and the nylon-6 crystallites (γ-form) have planar orientation, independent of montmorillonite content and the degree of orientation of nylon-6 crystallites increases with content of montmorillonite.[7] Additionally, detailed X-ray scattering of an injection-molded bar revealed the triple-layer structure consisting of surface, intermediate, and middle layers which have different preferred orientation; in the surface layer both the silicate monolayers and the chain axes of nylon-6 crystallites are parallel to the bar surface though the latter are randomly oriented within the plane, in the intermediate layer the silicate monolayers remain parallel to the bar surface but the nylon-6 crystallites rotate by 90° so that the chain axes would be perpendicular to the bar surface or the silicate monolayers, and in the middle layer the silicate monolayers are randomly oriented around the flow axis of the NCH bar while remaining parallel to it, and the nylon-6 crystallites are randomly oriented around the flow axis while keeping their chain axes perpendicular to the silicate monolayers.[8]

The objective of this study is to explore the three-dimensional structure of the NCH system with a zone-drawn film. Zone drawing was carried out by the movement of a zone heater along the draw direction at a constant speed. The heater provides a sharp temperature distribution, producing a stable neck which is subsequently propagated by movement of the zone heater at a constant speed. The orientation of the crystal, lamellar, and layered silicate is addressed through transmission electron microscopy and small- and wide-angle scattering patterns parallel and perpendicular to the draw direction.

Experimental Section

Materials and Film Drawing. Commercially available 5 (NCH5) wt % layered silicate/nylon-6 in-situ polymerized polymer/layered silicate nanocomposite (PLSN) materials were obtained from Ube Industries, Ltd. (Japan).[45] Ring-opening polymerization of ϵ-caprolactam initiated by pendant carboxylic acids on the surface of the modified montmorillonite reportedly results in approximately 50% (NCH5) of the nylon-6 chains tethered to the surface of the montmorillonite via ionic interaction of the primary ammonium cation.[45] The PLSNs were obtained as extruded pellets and dried under a vacuum at 70−80 °C for 12 h prior to compression into the ∼100 μm film under 3000 psi pressure. Zone drawing was carried out at ∼210 °C by moving a pair of narrow-band heaters [7 cm × 5 mm × 0.5 mm (length × width × thickness)] along the film. A compressed film of 7 cm length was drawn under tensions controlled by different dead weights on an Instron. The heat band speed was 10 mm/min. The final draw ratio controlled by the weights was up to ×4. The decrease in thickness was approximately proportional to the increase in length.

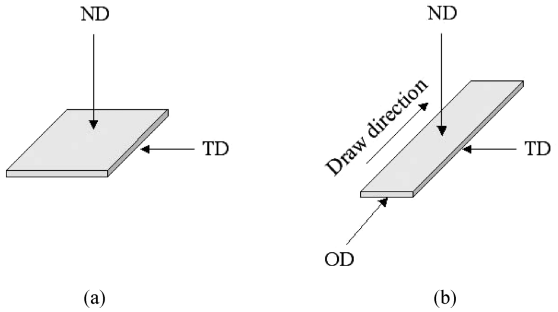

Figure 1. Directions of X-ray beams for structural analysis of (a) the biaxially protruded and (b) the drawn films. Normal direction, ND: normal to film surface; transverse direction, TD: perpendicular to normal (and drawing) direction; orthogonal direction, OD: parallel to the draw direction.

X-ray Characterization. Film specimens for the three-dimensional X-ray analysis were prepared by stacking the ∼1.5 mm wide films such that the X-ray specimen was ∼1 mm thickness. Figure 1 summarizes the interrelation between draw direction and scattering experiment. Wide-angle X-ray diffraction patterns were recorded on a phosphor image plate (Molecular Dynamics) in a Statton camera with the beam aligned (a) parallel to the draw direction (designated the OD pattern), (b) normal to the film surface (the ND pattern), and (c) perpendicular to both drawing and normal directions (the TD pattern). A Rigaku rotating anode X-ray generator, operated at 40 kV and 240 mA, produced Cu Kα radiation, which was then monochromated with the flat monochromator (Huber model 151). The sample-to-film distance was calibrated by SiO_2 powders. Synchrotron SAXS measurements were performed on Beamline 4C1 at Pohang Light Source (Korea) where a W/B4C double-multilayer monochromator delivered monochromatic X-rays with a wavelength (λ) of 0.1608 nm and a resolution of $\Delta\lambda/\lambda = 0.01$. A flat Au mirror was used to reject the higher harmonics from the beam. A 2-D CCD camera (Princeton Instruments Inc., SCX-TE/CCD-1242) was used to collect the scattered X-rays. The sample thickness was 1.0 mm, and the exposure time was approximately 1 min.

Transmission Electron Microscopy. Transmission electron microscopy (TEM) images were obtained using a Hitachi H-7600 microscope with an accelerating voltage of 100 kV. Ultrathin sections (∼70 nm) were prepared orthogonal to the film surface using an American Optical Ultracut microtome. In the case of the drawn film, the film was sectioned along the draw (OD) and transverse (TD) directions.

Results and Discussion

Biaxially Protruded Film. Figure 2 shows the wide-angle X-ray patterns at room temperature of the biaxially protruded NCH5 film. Isotropic rings were observed when the X-ray beam was perpendicular to the film surface (Figure 2a, ND) where as several arcs were observed when the X-ray beam was parallel to the film surface (Figure 2b, TD). These X-ray patterns indicated that there is a uniplanar orientation of crystallites in the biaxially protruded film. In contrast, the X-ray pattern of the pure nylon-6 film (without the layered silicate) made by the same method showed only isotropic rings associated with the α-phase when the X-ray beam was both parallel and perpendicular to the film surface, suggesting that the uniplanar orientation of crystallites

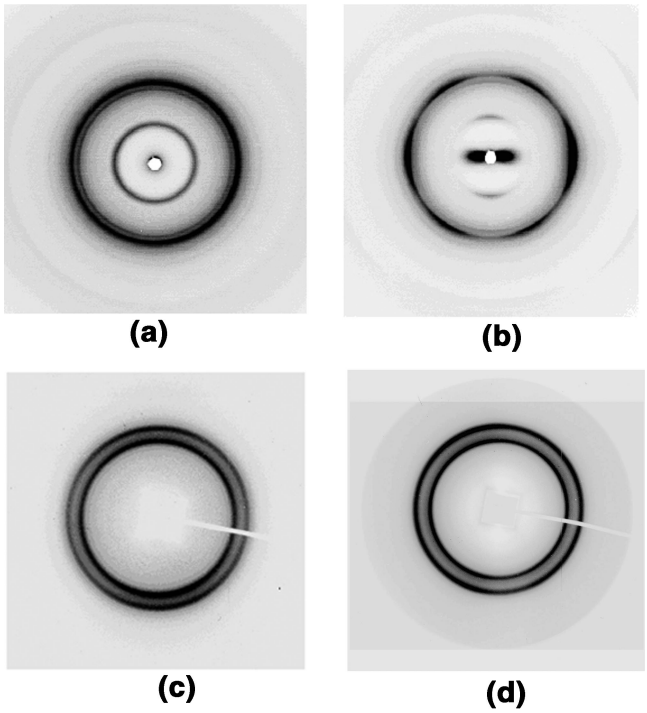

Figure 2. Wide-angle X-ray patterns of the biaxially protruded NCH5 film with an X-ray beam of (a) ND and (b) TD directions and of nylon-6 film with an X-ray beam (c) ND and (d) TD directions. For TD orientation, the vertical direction in the figure is parallel to the film surface. For NCH5, the central ring and arches of the first Bragg reflection arise from 020, whereas peripheral rings and arches arise from $\bar{2}01/200/001$ of the γ-crystal structure. For nylon-6, the two rings arise from 200 (inner ring) and 002 (outer ring) reflections of the α-crystal structure.

in pressed NCH5 film is due to the presence of the layered silicate (Figure 2c, ND; Figure 2d, TD).

As previously reported, the γ-form dominates the crystalline phase of the nylon-6 in the NCH5.[33,46] The first isotropic 020 Bragg reflection of the γ-form at d = 8.37 Å in Figure 2a is parallel to the film surface in Figure 2b. This indicates that the chain axis within the crystallites is oriented parallel to the film surface (the b axis is the chain axis). The γ-form has a pseudohexagonal structure in the ac basal plane, and the 001 and $\bar{2}01$[47,48] reflections are separated from the 200 reflection by +59° and −60°, respectively, in the azimuthal direction at the similar d-spacings; the d-spacings of $\bar{2}01$, 200, and 001 reflections based on the Arimoto's unit cell are 4.10, 4.11, and 4.00 Å, respectively.[49] The strong isotropic $\bar{2}01/200/001$[49] reflection of the γ-form at d = 4.21 Å in Figure 2a corresponds to six reflections, separated by approximately 60° along the azimuthal direction; in Figure 2b, the d-spacing increases from the calculated one and is known to change depending on the processing conditions.[50] Among the six reflections at $d \sim 4.2$ Å in Figure 2b, the intensity of the two reflections along the equator of the pattern (corresponding to reciprocal lattice vectors perpendicular to the film surface) is stronger than the other four reflections. If the reflections perpendicular to the film surface were indexed as 200 (or $001/\bar{2}01$), the other four reflections would be indexed as $001/\bar{2}01$(or 200). The assignment of the six reflections between 200 and $001/\bar{2}01$ cannot be determined. However, we know that either the bc or ab plane of the unit cell is parallel to the film surface. The weak and sharp reflection in the vertical direction at d = 4.52 Å is not 040 reflection (d_{040} = 4.18 Å) but the layered silicate's 020/110 reflection.[50] (Note that this reflection is present up to the maximum temperature examined, 280 °C, which is far above the melting temperature of the nylon-6 crystal.) The 00l reflections from the layered silicate other than 020/110 reflection were not observed due to the exfoliated structure. The vertical position of the 020/110 reflection also indicates that the surface of the clay is parallel to the film surface.

Figure 3 shows the small-angle X-ray patterns of the pressed NCH5 film. Weak and isotropic scattering is observed when the X-ray beam is perpendicular to the film surface (Figure 3a, ND), where as a strong streak along the equatorial direction (corresponding to reciprocal lattice vectors perpendicular to the film surface) is observed when the X-ray beam is incident parallel to the film surface (Figure 3b, TD). This streak arises from the large scattering density of the silicate layers oriented parallel to the film surface. For layered silicates oriented within the film, the scattering vector of the layered silicate is normal to the film surface and cannot touch the Ewald sphere when the X-ray beam is perpendicular to the film surface. The Herman's orientation parameter[19] determined from the azimuthal scan at $q = 0.3$ nm^{-1} was 0.81, indicating that the uniplanar orientation of the clay sheet is quite good.

A sector average along the equatorial streak (Figure 3c) indicates two small angle maxima at $q = \sim 0.145$ and ~ 0.29 nm^{-1} are present. The data are well described by two Gaussian functions and the background of the molten polymer with the form $a + bx^{-c}$. A possible explanation for these maxima is that the layered silicate (or some part of the layered silicate) has some regular spacing interval at ~43 nm as proposed in previous SAXS studies.[25] Transmission electron microscopy (discussed below) verifies extensive dispersion of the layered silicates and layer correlation between 40 and 50 nm. Another possible explanation for these SAXS features is crystal lamellar ordering. This supposition is strengthened from the observation that the strength of these maxima depends on process history and in some cases disappears at temperatures near the melting point of polymer crystallites ($T \sim 220$ °C).[51] However, the direction of these maxima implies that the lamellar ordering is perpendicular to the chain axis as shown in Figure 3b. Usually the lamellar ordering is parallel to the chain axis, and its periodicity, referred to as the long period, reflects the repeat distance between crystalline and amorphous regions.

Figure 4 shows a transmission electron micrograph of the pressed film sectioned along the thickness direction. The surface of the aluminosilicate layers is oriented parallel to the film surface. The inset shows the Fourier transform of the image showing a strong streak along the direction perpendicular to the film surface. This is similar to the small-angle scattering pattern, supporting the superposition that the small-angle scattering is due to the electron density difference between the layered silicate and the base resin. Detailed analysis of the intensity distribution along the streak for a variety of micrographs reveals a weak feature in the Fourier transform at 40−47 nm.

The combination of WAXS, SAXS, and TEM image indicates that the morphology in the biaxially protruded film has a uniplanar structure as shown in Figure 5; the exfoliated aluminosilicate layers are parallel to the film surface, and the crystals (mostly γ-form) are oriented with its bc (or ac) plane parallel to the film surface. Polymer chain direction within the crystallites

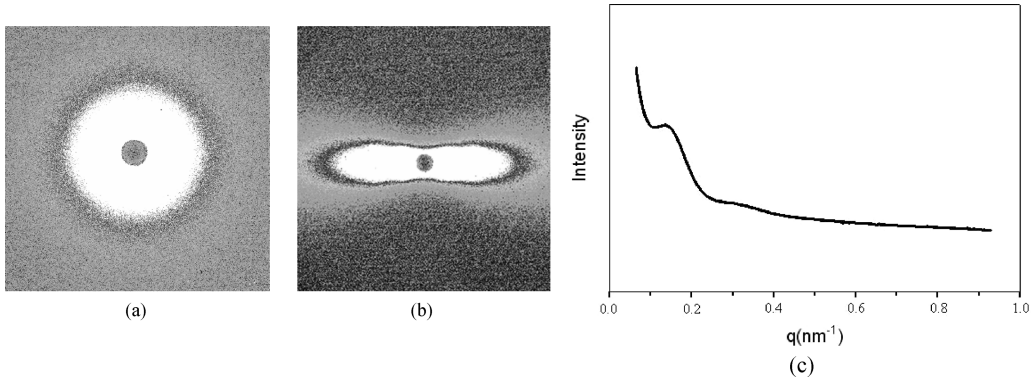

Figure 3. Small-angle X-ray patterns of the biaxially protruded film with an X-ray beam of (a) ND and (b) TD directions. A sector average along the equator in (b) reveal two small angle maximum displayed in (c) (solid line).

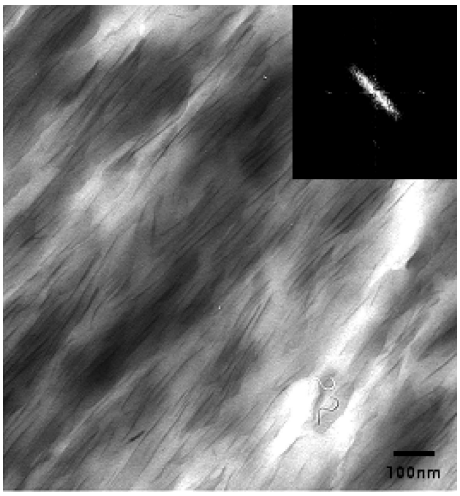

Figure 4. Transmission electron micrograph of the pressed film sectioned along the thickness direction.

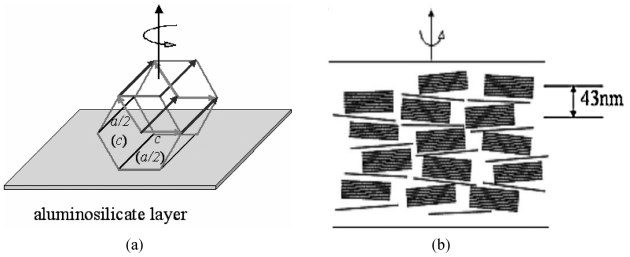

Figure 5. Morphological model of the biaxially protruded film: (a) the orientation of the γ-crystallite unit cell with respect to the aluminosilicate layer where the unit cell is close to hexagonal when the half of the a dimension is considered; (b) the orientation of the lamellar and aluminosilicate layers with respect to the film surface.

is in the b direction and parallel to the film surface. A large periodicity (~43 nm) perpendicular to the film surface is tentatively ascribed to a crystallite-layered silicate superstructure. This structure is similar to the skin region in the injection-molded samples which was studied by Kojima et al.[43]

Zone-Drawn Film. Figure 6 shows the wide-angle X-ray patterns of the ×4 drawn NCH5 film when the X-ray beam is along the three principal directions (ND, TD, and OD). Figure 6a (the ND pattern) corresponds to a typical fiber X-ray pattern with the draw direction is in the vertical direction. The 200 and 002 reflections of the α-phase at $d = 4.52$ Å and $d = 3.79$ Å are observed along the equator and straddle the $\bar{2}01/200/001$ reflections of the γ-phase. The presence of these two reflections indicates that the α-phase was produced during the drawing process, as commonly reported for drawing of γ-containing nylon-6 fibers.[52] The scattering from the layered silicates is barely discernible in the small angle region of Figure 6a, indicating that they remained oriented within the plane of the film. Similar to the ND direction, the TD direction (Figure 6b) also shows a typical uniaxial X-ray pattern. A strong streak along the equator in Figure 6b indicates that the original orientation of the layered silicates in the biaxially protruded film was maintained after drawing. The OD pattern (Figure 6c) shows $h0l$ reflections as well as the absence of the 020 reflection of the γ-phase. The latter implies that the chain axis within the γ-crystallites is parallel to the draw direction (note that the b axis is the chain axis). The positions of the 200 and 001 reflections of the γ-form are similar to that observed for the initial film (Figure 2b), indicating that the relative orientation between the layered silicate and the γ-form is maintained throughout drawing. The 200 and 002 reflections of the newly formed α-phase, however, are much more isotropic than compared to those of the γ-form. This result strongly suggests that the α-form crystallized during the drawing of the film and does not have an orientation correlation with the layered silicate. This is in accordance with Lincoln et al.'s claim that the crystallized site of the α-form is at a distance from the layered silicate.[19]

Figure 7 shows the corresponding small-angle X-ray patterns of the drawn NCH5 film when the X-ray beam is along the three principal directions (ND, TD, and OD). In contrast to the initial film, the ND pattern shows a small-angle maximum along the meridional direction and a streak along the equator. The small-angle maximum in the meridional direction increased with the draw ratio. In conjunction with wide-angle patterns this indicates that the α-form appears during drawing, with the chain axis parallel to the draw direction giving rise to the lamellar scattering along the meridian. The TD (Figure 7b) and OD (Figure 7c) patterns show strong equatorial streaks due to the planar orientation of the layered silicate. The approximate Herman's orientation parameter was 0.90 for TD and 0.85 for OD. The larger orientation parameter in the TD direction after drawing indicates that the uniaxial process further aligns the layers parallel to the film surface. However, the slightly lower value for the OD projection implies that additional ordering is not as extensive in the plane perpendicular to the draw direction. The twist in Figure 7c may be due to buckling or slight misalignment of the sample during preparation.

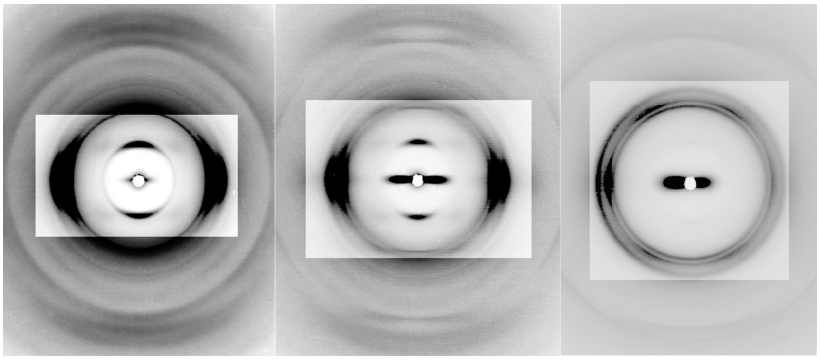

(a) (b) (c)

Figure 6. Wide-angle X-ray patterns of the drawn film with the X-ray beam along the (a) ND, (b) TD, and (c) OD directions; the vertical direction in (a) and (b) is the draw direction, and the horizontal direction in (c) is perpendicular to the film surface. The contrast of the central part of (a−c) is controlled for a better view.

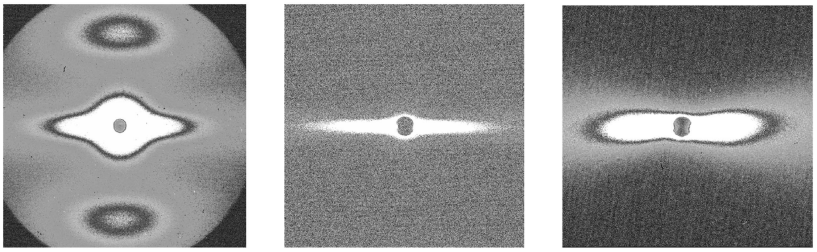

(a) (b) (c)

Figure 7. Small-angle X-ray patterns of the drawn film with an X-ray beam along the (a) ND, (b) TD, and (c) OD directions: the vertical direction in (a) and (b) is the draw direction, and the horizontal direction in (c) is perpendicular to the film surface.

Figure 8 shows transmission electron micrographs of the drawn film sectioned along the draw direction (Figure 8a, TD) and perpendicular to the draw direction (Figure 8b, OD). Figure 8a shows straightened parallel layers, similar to that of biaxially protruded film before drawing (Figure 4). In contrast, Figure 8b shows a wavy, buckled structure of the layered silicate, with the groove of the buckled structure along the draw direction. Fourier transforms of the images are shown in the insets and coincide with the small-angle scattering; the OD image (Figure 7c) shows azimuthally broad features while the TD image (Figure 7b) shows a narrow, straight streak. The scattering vector associated with the layer thickness, which is normal to the surface of the layered silicate, is oriented nearly perpendicular to the draw direction, and the projection along the TD direction is straight. In contrast, the same scattering vector has a wider distribution around the direction perpendicular to the film surface along the OD direction due to the buckled structure.

The combination of these two images indicates that the layered silicates buckle perpendicular to the draw direction. Compressive strain in this direction arises from the Poisson effect, which results in decreased sample thickness and width with increased deformation along the draw direction. The subsequent stress state within the plane of the film (tension along and compression perpendicular to the draw direction) leads to a buckling (wrinkling) failure of the layers that are oriented parallel to the film surface. This is analogous to the failure mode of a sheet of paper compressed in-plane from its edges. A montmorillonite layer does not have isotropic moduli. The in-plane tensile modulus, E_1, of montmorillonite has been estimated around 230 GPa[53] where as the transverse modulus is 4.1 times less (~56 GPa).[9] The failure mode appears to occur for a collection of aluminosilicate layers (2−4) and not individually. For example, in the upper left corner of Figure 8b, sheets that are in relatively close proximity

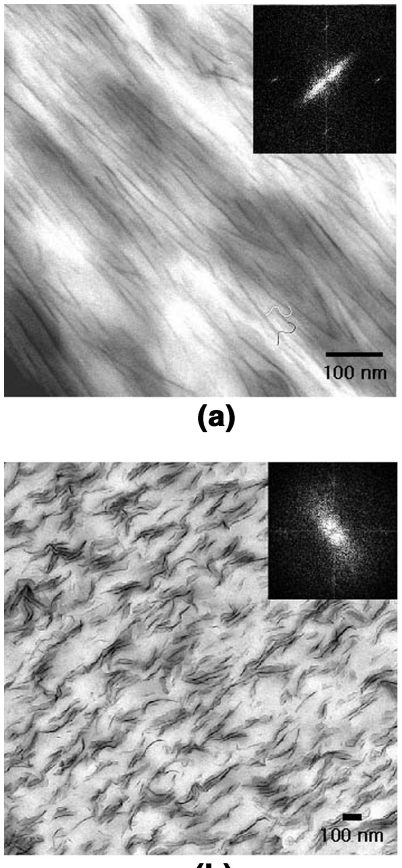

Figure 8. Transmission electron micrographs of the drawn film sectioned along the (a) TD direction and (b) OD direction.

exhibit the same buckling wavelength, and the extent of out-of-plane buckling is on the order of the spacing between sheets. This indicates that the local failure of these layered silicates occurred simultaneously and as a group. Conceptually, this is similar to recent conclusions by Boyce and co-workers[54] derived from computer simulations of small-scale uniaxial deformation of a two-dimensional, aligned arrangement of rods representing a unilamellar arrangement of layered silicates. Here, rods in close proximity effectively shielded the intervening matrix, reducing local matrix strain. The local strain and stress fields implied these groupings of rods acted as an "effective" reinforcement particle. Further analysis of the wavelength of the wrinkle and onset of the buckling failure mode will provide critical information on the local mechanics around the layered silicate sheet and combined with computer simulations and detailed particle distribution analysis will provide quantitative determination of the local stress distribution and strength of the mechanical coupling between the layered silicate and polymer.

Conclusion

The quenched biaxially protruded films exhibited a uniplanar crystalline texture with the *b*-axis of the dominate γ-form oriented toward the normal to the film surface and the surface of the layered silicate oriented parallel to the film surface. Small-angle scattering features suggest that the lamellar of the γ-form is within the proximity of the layered silicate and has a fringed micelle structure. Upon uniaxial drawing, α-crystallites developed with a lamellar regularity of $\sim$15 nm along the draw direction, comparable to previous studies on pure nylon-6 fibers. The newly formed α-form exhibited a uniaxial texture with the *b*-axis parallel to the draw direction. This suggests that the α-form crystallized during the drawing of the film and does not have an orientation correlation with the layered silicate. Finally, the layered silicate within the zone-drawn film buckled perpendicular to the draw direction, analogous to failure of a uniaxially strained sheet of paper. The failure mode appears to occur for a collection of parallel aluminosilicate layers (2−4), implying that the layers do not act independently as reinforcement. Recognition of the structural changes of the layered silicate and crystalline regions in response to uniaxial deformation of planar oriented films is critical to ascertaining the local transport properties of shaped layered silicate nanocomposite parts.

Detailed morphology characterization of these hierarchical composite systems and novel methods to controllably deform the structure, such as zone refining, are paramount to establishing the critical parameters impacting structure−property relationships. The specific crystallite orientation and impact of deformation on polymorphism and mesostructure provide more precise details to begin to understand applicability as well as deviations from models of local transport and permeability based on a featureless medium with rigid plates. Further evaluation of the latter is key to quality control of these process-history-sensitive nanocomposites as well as ascertaining the feasibility of extending nanocomposites to piezo-responsive smart membranes.

Acknowledgment. This work was supported by a Grant from the Korean Research Foundation (KRF-041-D00199) and the Brain Korea 21 Project. R.A.V. appreciates the fruitful discussions with H. Koerner and L. Drummy. This work was supported in part by the Ministry of Science & Technology (MOST), by POSCO, by the Center for Integrated Molecular System (Korea Science & Engineering Foundation), and by the KISTEP (Basic Research Grant of Nuclear Energy, MOST).

References and Notes

(1) Giannelis, E. P. *J. Mineral. Metals Mater. Soc.* **1992**, March, 28.
(2) Okada, A.; Kawasumi, M.; Usuki, A.; Kojima, Y.; Kurauchi, T.; Kamigaito, O. *Mater. Res. Soc. Symp. Proc.* **1990**, *171*, 45.
(3) Usuki, A.; Kojima, Y.; Kawasumi, M.; Okada, A.; Kurauchi, T.; Kamigaito, O.; Deguchi, R. *Polym. Prepr. Jpn.* **1990**, *39*, 2427.
(4) Kojima, Y.; Okada, A.; Usuki, A.; Kawasumi, M.; Kurauchi, T.; Kamigaito, O.; Deguchi, R. *Polym. Prepr. Jpn.* **1990**, *39*, 2430.
(5) Kojima, Y.; Okada, A.; Kawasumi, M.; Okada, A.; Fukushima, Y.; Kurauchi, T.; Kamigaito, O. *J. Mater. Res.* **1993**, *8*, 1185.
(6) Usuki, A.; Koiwai, A.; Kojima, Y.; Kawasumi, M.; Okada, A.; Kurauchi, T.; Kamigaito, O. *J. Appl. Polym. Sci.* **1995**, *55*, 119.
(7) Kojima, Y.; Usuki, A.; Kawasumi, M.; Odaka, A.; Kurauchi, T.; Kamigaito, O.; Kaji, K. *J. Polym. Sci., Part B: Polym. Phys.* **1994**, *32*, 625.
(8) Kojima, Y.; Usuki, A.; Kawasumi, M.; Okada, A.; Kurauchi, T.; Kamigaito, O.; Kaji, K. *J. Polym. Sci., Part B: Polym. Phys.* **1995**, *33*, 1039.
(9) Ke, Y.; Long, C.; Qi, Z. *J. Appl. Polym. Sci.* **1999**, *71*, 1139.
(10) Messersmith, P. B.; Giannelis, E. P. *J. Polym. Sci., Part A: Polym. Chem.* **1995**, *33*, 1047.
(11) Vaia, R. A.; Price, G.; Ruth, P. N.; Nguyen, H. T.; Lichtenhan, J. *Appl. Clay Sci.* **1999**, *15*, 67.
(12) Kojima, Y.; Usuki, A.; Kawasumi, M.; Okada, A.; Kurauchi, T.; Kamigaito, O. *J. Appl. Polym. Sci.* **1993**, *49*, 1259.
(13) Krishnamoorti, R.; Giannelis, E. P. *Macromolecules* **1997**, *30*, 4097.
(14) VanderHart, D. L.; Asano, A.; Gilman, J. W. *Chem. Mater.* **2001**, *13*, 3781.
(15) Tseng, C. R.; Wu, S. C.; Wu, J. J.; Chang, F. C. *J. Appl. Polym. Sci.* **2002**, *86*, 2492.
(16) Strawhecker, K.; Manias, E. *Chem. Mater.* **2000**, *12*, 2943.
(17) (a) Han, B.; Ji, G.; Wu, S.; Shen, J. *Eur. Polym. J.* **2003**, *39*, 1641. (b) Yu, Z. Z.; Yang, M.; Zhang, Q.; Zhao, C.; Mai, Y. W. *J. Polym. Sci., Part B: Polym. Phys.* **2003**, *41*, 1234. (c) Liu, X.; Wu. Q.; Berglund, L. A. *Polymer* **2002**, *43*, 4967.
(18) (a) Liu, Z.; Zhou, P.; Yan, D. *J. Appl. Polym. Sci.* **2004**, *91*, 1834. (b) Zhang, G.; Yan, D. *J. Appl. Polym. Sci.* **2003**, *88*, 2181. (c) Wang, L.; He, S.; Hao, L.; Zhu, C.; Qi, Z. *Gaofenzi Cailiao Kexue Yu Gongcheng* **2002**, *18*, 62.
(19) Lincoln, D. M.; Vaia, R. A.; Wang, Z. G.; Hsiao, B. S.; Krishnamoorti, R. *Polymer* **2001**, *42*, 9975.
(20) Liu, X.; Wu, Q.; Berglund, L. A.; Qi, Z. *Macromol. Mater. Eng.* **2002**, *287*, 515.
(21) Wu, T. M.; Chen, E. C.; Liao, C. S. *Polym. Eng. Sci.* **2002**, *42*, 1141.
(22) Nam, P. H.; Maiti, P.; Okamoto, M.; Kotaka, T.; Hasegawa, N.; Usuki, A. *Polymer* **2001**, *42*, 9633.
(23) Ke, Y.; Long, C.; Qi, Z. *J. Appl. Polym. Sci.* **1999**, *71*, 1139.
(24) Strawhecker, K.; Manias, E. *Chem. Mater.* **2000**, *12*, 2943.
(25) Devaux, E.; Bourbigot, S.; El, A. *J. Appl. Polym. Sci.* **2002**, *86*, 2416.
(26) Krikorian, V.; Kurian, M.; Galvin, M. E.; Nowak, A. P.; Deming, T. J.; Pochan, D. J. *J. Polym. Sci., Part B: Polym. Phys.* **2002**, *40*, 2579.
(27) Carter, C. M. *Annu. Tech. Conf.—Soc. Plast. Eng.* **2001**, *59*, 3210.
(28) Wu, T. M.; Chen, E. C.; Liao, C. S. *Polym. Eng. Sci.* **2002**, *42*, 1141.
(29) Wu, T. M.; Wu, J. Y. *J. Macromol. Sci., Phys.* **2002**, *B41*, 17.
(30) Fornes, T. D.; Paul, D. R. *Polymer* **2003**, *44,* 3945.
(31) Tseng, C. R.; Wu, S. C.; Wu, J. J.; Chang, F. C. *J. Appl. Polym. Sci.* **2002**, *86*, 2492.
(32) Wu, H. D.; Tseng, C. R.; Chang, F. C. *Macromolecules* **2001**, *34*, 2992.
(33) Wu, Q.; Liu, X.; Berglund, L. A. *Macromol. Rapid Commun.* **2001**, *22*, 1438.
(34) Brill, R. *Z. Phys. Chem. B* **1943**, *53*, 61.

(35) Holmes, R.; Bunn, D. W.; Smith, D. L. *J. Polym. Sci.* **1955**, *17*, 619.
(36) Arimoto, H.; Ishibashi, M.; Hirai, M.; Chatani, Y. *J. Polym. Sci., Part A: Polym. Chem.* **1965**, *3*, 317.
(37) Bradbury, E. M.; Brown, L.; Elliot, A.; Parry, D. A. D. *Polymer* **1965**, *6*, 465.
(38) Samon, J. M.; Schultz, J. M.; Wu, J.; Hsiao, B.; Yeh, F.; Kolb, R. *J. Polym. Sci., Part B: Polym. Phys.* **1999**, *37*, 1277.
(39) Ho, J.; Wei, K. *Macromolecules* **2000**, *33*, 5181.
(40) Dasgupta, S.; Hammond, W.; Goddard III, W. *J. Am. Chem. Soc.* **1996**, *118*, 12291.
(41) Kinoshita, Y. *Makromol. Chem.* **1959**, *33*, 1.
(42) Mathias, L.; Davis, R.; Jarrett, W. *Macromolecules* **1999**, *32*, 7958.
(43) Kojima, Y.; Matsuoka, T.; Takahashi, H.; Kurauchi, T. *J. Appl. Polym. Sci.* **1994**, *51*, 683.
(44) Liu, L.; Qi, Z.; Zhu, X. *J. Appl. Polym. Sci.* **1999**, *71*, 1133.
(45) Usuki, A.; Kojima, Y.; Kawasumi, M.; Okada, A.; Kukushima, Y.; Kurauchi, T.; Kamigaito, O. *J. Mater. Res.* **1993**, *8*, 1179.
(46) Liu, X.; Wu, Q. *Polymer* **2002**, *43*, 1933.
(47) Some references index this reflection as 201 instead of $\bar{2}01$, which may be mistyping.[48]
(48) Murthy, N. S.; Aharoni, S. M.; Szollosi, A. B. *J. Polym. Sci., Part B: Polym. Phys.* **1985**, *23*, 2549.
(49) Arimoto, H.; Ishibashi, M.; Chatani, Y. *J. Polym. Sci., Part A* **1965**, *3*, 317.
(50) Medellin-Rodriguez, F. J.; Hsiao, B. S.; Chu, B.; Fu, B. X. *J. Macromol. Sci., Part B: Phys.* **2003**, *42*, 201.
(51) Manuscript in preparation.
(52) Samon, J. M.; Schultz, J. M.; Hsiao, B. S. *Polymer* **2000**, *41*, 2169.
(53) Manevitch, O. L.; Rutledge, G. C. *J. Phys. Chem. B* **2004**, *108*, 1428.
(54) Sheng, N.; Boyce, M. C.; Park, D. M.; Rutledge, G. C.; Abes, J. I.; Cohen, R. E. *Polymer* **2004**, *45*, 487.

MA048258N